



In situ formed vanadium-oxide cathode coatings for selective hydrogen production



Balázs Endrődi^{a,b,*}, Vera Smulders^c, Nina Simic^d, Mats Wildlock^d, Guido Mul^c, Bastian Mei^c, Ann Cornell^a

^a Applied Electrochemistry, School of Engineering Sciences in Chemistry, Biotechnology and Health, KTH Royal Institute of Technology, SE 100-44, Stockholm, Sweden

^b Department of Physical Chemistry and Materials Science, University of Szeged, Rerrich B. square 1, H-6720, Szeged, Hungary

^c PhotoCatalytic Synthesis Group, MESA + Institute for Nanotechnology, Faculty of Science and Technology, University of Twente, Meander 229, P.O. Box 217, 7500 AE, Enschede, the Netherlands

^d Nouryon, SE 445-80, Bohus, Sweden

ARTICLE INFO

Keywords:

Hydrogen evolution reaction
Cathode selectivity
Overall water splitting
Industrial chemistry
Chlorate electrolysis

ABSTRACT

Electrode selectivity towards hydrogen production is essential in various conversion technologies for renewable energy, as well as in different industrial processes, such as the electrochemical production of sodium chloride. In this study we present sodium metavanadate as a solution additive, inducing selective cathodic formation of hydrogen in the presence of various other reducible species such as hypochlorite, chloride, oxygen, nitrate, hydrogen-peroxide and ferricyanide. During electrolysis a vanadium-oxide coating forms from the reduction of sodium metavanadate, explaining the observed enhanced selectivity. The hydrogen evolution reaction proceeds without significantly altered kinetics on such in situ modified electrode surfaces. This suggests that the reaction takes place at the interface between the electrode surface and the protective film, which acts as a diffusion barrier preventing the unwanted species to reach the electrode surface.

1. Introduction

With the continuously increasing contribution of renewables to the total energy mix, a solution must be found to cope with the intermittency of these energy sources [1]. Currently, among the promising avenues, storing the excess energy in the form of high energy density chemicals has gained significant attention. Together with different products derived from the reduction of CO_2 (e.g. CH_3OH , CO , CH_4) [2,3], hydrogen is an important future energy carrier [4].

One particularly promising way to form hydrogen is through the photocatalytic splitting of water to hydrogen and oxygen, directly harnessing solar energy [5]. Although this process can be driven on a single semiconductor material with proper conduction and valence band positions, transition metal oxide or noble metal co-catalysts are typically applied to reach reasonable reaction rates [6,7]. On these co-catalysts (such as Pt), the unfavorable reduction of in situ formed oxygen, inducing back-reaction of hydrogen to water, however decreases the production rates. Strategies to avoid oxygen reduction and these losses include the development of protective coatings, hindering

the transport of oxygen to the co-catalyst surface. Such membrane like behavior was reported for different amorphous oxides, e.g. titanium dioxide [8], nickel oxide [9,10], silicon dioxide [11–13], molybdenum oxide [13,14] or chromium oxide [15–17]. Studying the performance of such coatings by electrochemical techniques, the hydrogen evolution reaction (HER) was shown to proceed selectively, while other cathodic processes were hindered [18]. As it was summarized recently by Esposito, buried catalyst surfaces hold a great potential for the rational design of active and stable catalysts for various applications, including photochemical and electrochemical water splitting [19]. Further, poisoning (by CO for example), and sintering of metal particles are also suppressed, hence improving catalyst stability. To further emphasize the general applicability of buried catalysts we also mention that MnO_x layers were shown to increase the selectivity of IrO_2 in anodic oxygen formation in aqueous brine solutions, by disfavoring the transport of chloride to the electrode surface [20].

Selective hydrogen production is of prime importance for the industrial electrolytic production of sodium chloride. In the process a concentrated brine solution is electrolyzed using dimensionally stable

Abbreviations: RDE, rotating disk electrode; HER, hydrogen evolution reaction; ORR, oxygen reduction reaction; RPM, rotation per minute; EQCM, electrochemical quartz crystal microbalance; DSA, dimensionally stable anode; CV, cyclic voltammetry

* Corresponding author.

E-mail address: endrodi@kth.se (B. Endrődi).

<https://doi.org/10.1016/j.apcatb.2018.11.038>

Received 4 September 2018; Received in revised form 5 November 2018; Accepted 14 November 2018

Available online 16 November 2018

0926-3373/© 2018 The Authors. Published by Elsevier B.V. This is an open access article under the CC BY license (<http://creativecommons.org/licenses/by/4.0/>).

anodes (DSAs) and low carbon steel cathodes in undivided electrochemical cells [21–23]. Chlorine forms at the anode, and hydrolyses to hypochlorite, which reacts to chlorate in the electrolyte bulk. The Faradaic efficiency of HER is lowered by several parasitic reactions, most importantly by the reduction of the hypochlorite intermediate and of chlorate ions.

Currently, high process efficiency is achieved by the addition of $\text{Na}_2\text{Cr}_2\text{O}_7$ to the electrolyte [24]. During electrolysis a thin Cr(III)-oxide/hydroxide layer deposits on the cathode, practically eliminating the cathodic reactions leading to losses [25–31]. Importantly, the chemical nature of the formed layer is likely similar to that of the protective chromium oxide coatings in the case of photocatalytic water splitting [15–17]. This suggests a similar reason behind the increased process efficiency in the two very different scenarios. It should be mentioned that in the chlorate process, the chromium(VI) in the solution is also required for buffering the electrolyte [32], and to increase the decomposition rate of hypochlorite in the solution [33–35].

Several attempts were made to replace the carcinogenic, mutagenic and reprotoxic chromium(VI) compounds [24]. Rare earth metal salts [36] and molybdate [37–39] were both shown to increase HER efficiency, but their use is hampered by (1) their low solubility in high ionic strength solutions, or (2) an increased anodic formation of oxygen, respectively. Most recently we presented permanganate as a promising alternative additive [40]. Unfortunately, the depositing MnO_x film thickens continuously, preventing the industrial use of such permanganate additive.

Vanadium offers a versatile redox chemistry that is very often exploited in redox-flow batteries [41,42]. Vanadium species were also proven to be potential candidates in chromium-free corrosion protection layers [43–45]. Similarly to the chromate coatings, a vanadium oxide film forms on the electrode (e.g. Al) surface when it is treated with e.g. NaVO_3 solution. This leads to a lowered corrosion rate while having little effect on the HER. Moreover, it was also shown earlier that HER proceeds on ex situ formed vanadium oxide electrodes [46].

In this study, we demonstrate – guided by recent developments in photocatalysis and electrochemistry – that electrode coatings formed in situ by reduction of sodium metavanadate lead to the suppression of various unwanted cathodic processes, such as the reduction of dissolved oxygen or hypochlorite. On the other hand, the HER proceeds on the modified electrode surface without significantly altered kinetics. These results are highly relevant in photocatalysis and particularly for electrochemical chlorate production evidencing that buried catalysts can be produced using VO_x coatings.

2. Materials and methods

2.1. Chemicals used

NaOCl (0.5 M solution in 0.1 M NaOH), NaVO_3 , $\text{K}_3\text{Fe}(\text{CN})_6$, H_2O_2 , NaNO_3 , NaCl , NaClO_4 , NaOH and HCl (37% solution) were purchased from VWR International and used as received. The sodium chlorate was provided by Nouryon and was purified by recrystallization. Commercially available buffer solutions of $\text{pH} = 4.00$ and 7.00 from Metrohm were used to calibrate the pH meter (Metrohm 827 pH lab instrument or Metrohm 907 Titando titrator equipped with a Unitrode Pt 1000 combined pH and temperature sensor) prior to each experiment. The pH values are reported as read from the instrument calibrated to these buffers. Millipore Direct-Q 3 UV instrument was used to prepare all solutions. We note here, that at the neutral pH of the chlorate electrolyte, both hypochlorous acid and its deprotonated form, hypochlorite ions are present in the solution; the total concentration of these species is denoted as “hypochlorite” for simplicity.

2.2. Electrochemical measurements

All the cyclic voltammetry (CV) and polarization curve measurements were performed using a Princeton Applied Research PAR273 A type instrument. In the classical 3 electrode electrochemical cell a $d = 4\text{ mm}$ Pt, glassy carbon or Fe rotating disk electrode (RDE) was used as working electrode, while a Pt cage and a $\text{Ag}/\text{AgCl}/\text{sat. KCl}$ ($E = +197\text{ mV}$ vs. SHE) served as counter and reference electrodes, respectively. The potentials in the followings are given with respect to the used reference electrode. The rotation rate (in rotation per minute (RPM)) was regulated using an Ametek 616 A type instrument. Before each measurement, the RDEs were polished on $1\text{ }\mu\text{m}$ sized alumina powder (Buehler Micropolish II). The residues of the polishing material were removed by treating the electrode in an ultrasonic bath in deionized water for 1 min. To rule out the unlikely contribution of any Pt contamination in the deposited vanadium oxide layers [47], some of the experiments were repeated using a Ti or graphite counter electrode. These experiments led to the exact same results as the ones performed using a Pt counter electrode. Also note, that for all our measurements a Pt electrode was used as reference, on which all of the unwanted reduction reactions are shown to proceed with fast kinetics.

The polarization curves were recorded in galvanostatic mode and were corrected for IR-drop using the current-interruption technique [48]; the electrode was polarized for 15 s at the given current density, and then the current was interrupted. The decay of the potential was measured for $500\text{ }\mu\text{s}$ with a time resolution of $1\text{ }\mu\text{s}$ using a National Instrument cDAQ-9172 device. The IR-corrected potential value was determined after fitting the experimental data with a third order polynomial, using Matlab. The measurements were performed between $j = -1 - -1000\text{ mA cm}^{-2}$, at 10 current levels / decade. The polarization curves were recorded both starting with the lowest current density and gradually increasing it, and vice versa. Before the measurements, the electrodes were polarized at the first applied current density for 100 s.

2.3. Electrochemical quartz crystal microbalance (EQCM) measurements

EQCM measurements were performed using a Gamry eQCM10 M module and a Biologic VSP potentiostat. Pt- or Au-coated QCM crystals (5 MHz, Q-sense) were used as working electrode, a custom-made $\text{Ag}/\text{AgCl}/3\text{ M NaCl}$, and a Pt wire ($d = 4\text{ mm}$, $L = 15\text{ cm}$, Alfa Aesar, > 99.99% purity) were used as reference and counter electrode, respectively. The electrolyte was degassed using N_2 for 1 h before the measurement and the cell was maintained at 288 K before and during the experiments using a thermostat bath. The CVs were recorded after the system was kept near the open circuit potential of $E = 0.5\text{ V}$ for 10 s, and then sweeping in a reductive direction to $E = -1.2\text{ V}$ at $\nu = 10\text{ mV s}^{-1}$, directly followed by an oxidative sweep to $E = +1.5\text{ V}$ at $\nu = 10\text{ mV s}^{-1}$, before returning to the starting potential.

2.4. Current efficiency measurements

The current efficiency measurements were performed in a custom-designed, undivided electrochemical cell using a mass spectrometer to analyze the cell off-gas. The details of the experimental setup are given elsewhere [40]. Briefly, the cell was completely closed by a tightly fitting lid. The solution was purged with a constant flow ($50\text{ cm}^3\text{ min}^{-1}$) of argon gas, which carried the formed gaseous products to a mass spectrometer (Hiden HPR-20, equipped with a quartz capillary inlet). The pH was kept constant by titration of 2 M NaOH or 6 M HCl solutions. The solution temperature was regulated by circulating water from an external heater in the jacket of the cell. Before each experiment, the mass spectrometer was calibrated for H_2 and O_2 by electrolyzing a 1 M NaOH solution at a constant current ($I = -300\text{ mA}$) using Pt working and counter electrodes. The hypochlorite concentration was determined by UV-vis spectroscopy

(Expedeon VersaWave instrument, $l = 1.000$ cm quartz cuvette). To quantify the HER efficiency, the hydrogen production rate was calculated from the flow-rate and the hydrogen content of the cell off-gas, determined by the mass spectrometer. The HER efficiency was then determined as the ratio between the measured H_2 production rate and the maximum H_2 production rate, calculated using Faraday's law, assuming 100% current efficiency for hydrogen production.

2.5. Kinetic studies on the homogeneous decomposition of hypochlorite

The homogeneous decomposition of hypochlorite was studied in the same setup as the current efficiency measurements (without electrodes). The mass spectrometer was calibrated for N_2 and O_2 by a mixture of argon and technical air ($50\text{ cm}^3\text{ min}^{-1}$ Ar + $3\text{ cm}^3\text{ min}^{-1}$ technical air). The hypochlorite solution was heated to $T = 80^\circ\text{C}$, while its pH was kept at $\text{pH} \approx 12$ to minimize the decomposition rate. The reaction was initiated by adding 6 M HCl until reaching $\text{pH} = 6.5$, which was kept constant using 2 M NaOH. Liquid samples were taken at regular time intervals to measure the hypochlorite concentration, while the O_2 content of the cell off-gas was continuously monitored using mass spectrometry. The measurements were performed in a 5.2 M NaClO_3 , 1.9 M NaCl and 80 mM NaClO containing solution – a composition close to the industrial chlorate electrolyte.

2.6. Compositional analysis by X-ray photoelectron spectroscopy (XPS)

For the XPS measurements, a vanadium oxide layer was deposited on an Au foil (0.05 mm thickness, Alfa Aesar, > 99.95%), which was first polished using 1.0 and 0.3 μm MicroPolish (Buehler) alumina, then roughened by potential cycling in a 0.1 M NaCl solution at 500 mV s^{-1} sweep rate from -0.26 V (holding for 1.3 s) to $+1.24\text{ V}$ (holding for 30 s), and repeating this 25 times. The film was deposited from 2 mM NaVO_3 containing 2 M NaCl solution for 30 min at $E = -2\text{ V}$ (using a Pt mesh counter, and a $\text{Ag}/\text{AgCl}/3\text{ M NaCl}$ reference electrode). The samples were then carefully rinsed using milliQ water and dried using N_2 stream.

The XPS measurements were performed on a Quantera SXM (Physical Electronics) instrument, equipped with an Al $\text{K}\alpha$ X-ray source (1486.6 eV). The binding energies were referenced to the C 1 s core level peak at 285 eV.

3. Results and discussion

3.1. Applicability of vanadate additive in the chlorate process

3.1.1. Effect of vanadate addition on the electrochemical reduction of hypochlorite

Hypochlorite is an essential intermediate in the chlorate process and generally an interesting compound to study electrochemical selectivity due to its reactivity. At industrial conditions, i.e. $\text{pH} = 6.5$, both the protonated, hypochlorous acid, and the deprotonated form, hypochlorite ions are present in the electrolyte. As the electrochemical reduction of hypochlorite is a diffusion limited process [40], two consecutive cathodic current plateaus are observed in the CVs in the absence of sodium metavanadate (between $+0.5\text{ V}$ – -0.2 V and -0.4 V – -1.2 V , marked with I and II in Fig. 1A) using a Pt RDE as cathode. The addition of sodium metavanadate leads to significant changes in the shape of the voltammograms. During the cathodic half-cycle (from the anodic endpoint towards more negative potential values), a decrease in the hypochlorite reduction current can be observed; the extent of the decrease scales with the added vanadate concentration. During the anodic sweep (upper curves), a more striking difference can be observed and at high enough additive concentration (above 500 μM) the hypochlorite reduction is almost completely suppressed in the potential range from $E = -1\text{ V}$ to -0.35 V . Nevertheless, hypochlorite reduction occurs above $E \approx -0.35\text{ V}$ indicated by a rapid cathodic

current increase.

Performing CV experiments in a solution with constant vanadate concentration (Fig. 1B) a more pronounced hindering of the hypochlorite reduction can be observed at low sweep rates; in anodic sweep direction almost no hypochlorite reduction is seen up to $E = -0.35\text{ V}$. The independence of this potential on the sweep rate suggests a surface confined electrochemical process, terminating the suppression of hypochlorite reduction. Finally, measurements at elevated temperature (Fig. S1A) and with an iron RDE (Fig. S1B) – to better resemble the industrial process – also confirmed these conclusions.

These observations are all in line with a slow, thin film deposition at very negative potential [49], and its oxidative dissolution at $E \approx -0.35\text{ V}$, hence restoring the original Pt electrode surface on which hypochlorite reduction readily takes place. This assumption is supported by EQCM measurements, where the mass change was traced during the course of a CV experiment (Fig. 2, Fig. S2-4). During the cathodic sweep in the presence of NaVO_3 a weight decrease is seen from $E \approx -0.3\text{ V}$, related to the reduction of platinum oxide, as proven by measurements performed in a limited potential range, avoiding the oxidation of the Pt substrate (Fig. S2D) [50]. A subsequent mass increase is observed starting from $E \approx -0.5\text{ V}$ (Fig. 2), which is absent for NaVO_3 -free electrolytes (Fig. S2A). Retaining the cathodic potential for longer time (Fig. S3A), the film growth is not immediately terminated and thicker films are obtained during constant cathodic polarization at negative potentials. In the reverse scan, an oxidation process is observed starting again at $E \approx -0.5\text{ V}$, followed by the decrease of the electrode mass to the initial value, showing the oxidative dissolution of the deposit. A similar film growth and dissolution behavior is observed during subsequent cycling (Fig. S2C). However, for the first cycle a slightly different behavior was observed, and film dissolution appears to be not entirely complete. Instead $\sim 1\text{ }\mu\text{g cm}^{-2}$ (less than a monolayer) remained on the surface (Fig. S2B). The total mass gained during the first cycle is $2.15\text{ }\mu\text{g cm}^{-2}$, ending in a saturation value at more negative potentials, indicating the deposition of a layer with an estimated thickness of 3–4 nm. Similar experiments performed with Au-coated EQCM electrodes suggest that a thicker film is deposited already at less negative potentials (Fig. S4). As for the Pt-coated electrodes, deposition on Au appears to be almost reversible.

The composition of the deposited layers was analyzed by XPS measurements (Fig. S5), where the presence of V^{3+} and V^{4+} oxidation states was confirmed [51], indicating that the deposit is most probably V_2O_3 , which is partially oxidized when exposed to air during sample transfer.

3.1.2. HER kinetics in the presence of vanadate

The kinetics of the HER in NaOCl -containing electrolyte was studied by recording IR-corrected polarization curves (Fig. 3 and Fig. S6). In the absence of vanadate two consecutive diffusion limited processes can be observed as sudden potential drops, related to the reduction of hypochlorite ions and hypochlorous acid (marked with I and II, similarly to the CVs in Fig. 1) [40]. This is followed by a linear region related to the HER. In the presence of vanadate this linear HER region is extended to significantly lower current densities, indicating a largely suppressed hypochlorite reduction in accordance with the CV measurements (Fig. 1). The polarization curve is shifted towards more negative potentials by ca. 40–50 mV, but similar HER Tafel-slopes are obtained in the absence and presence of the vanadate additive, indicating that the hydrogen evolution proceeds on the modified electrode surface without significantly altered kinetics. This conclusion is further strengthened by performing measurements in a hypochlorite free solution (Fig. S7), where an almost identical Tafel-slope and HER overpotential was observed in the presence and absence of vanadate.

Interestingly, for IR-corrected polarization curves recorded in the increasing current direction (Fig. S6A,B) no significant difference can be seen from the vanadate free case. This is in agreement with the EQCM measurements (Fig. 2), where the layer formation was observed

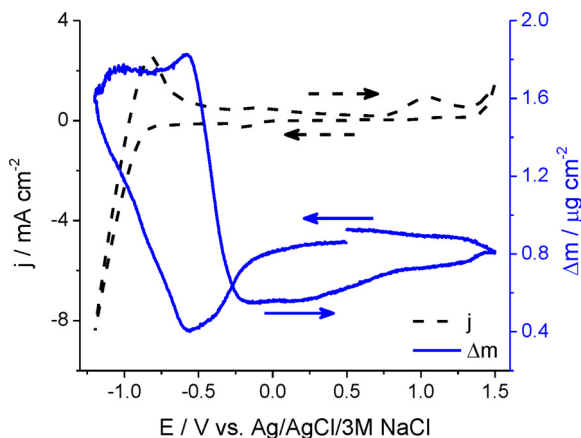
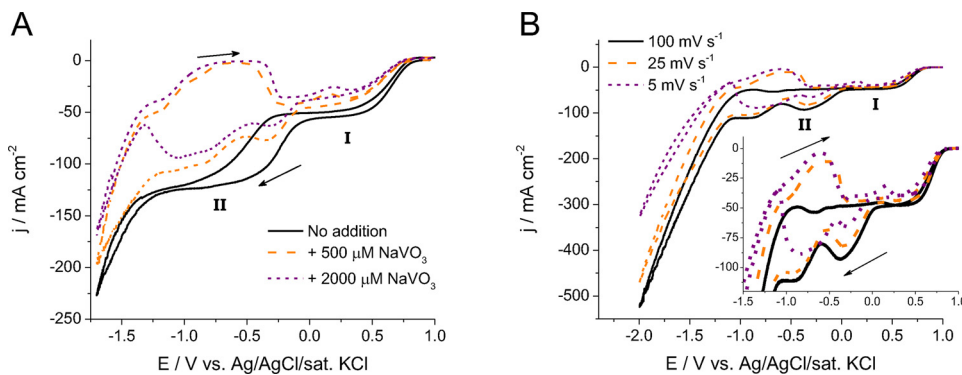


Fig. 2. The current response and mass change during the second cycle of a cyclic voltammetric measurement on a Pt-coated EQCM electrode, $T = 288 \text{ K}$, $\nu = 10 \text{ mV s}^{-1}$, and $\text{pH} = 6.5$ in a 2 M NaClO_4 solution containing 2 mM NaVO_3 .

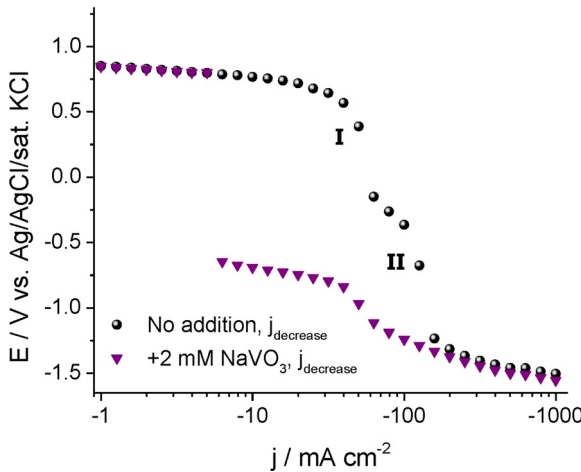


Fig. 3. IR-corrected polarization curves recorded in an $80 \text{ mM NaOCl} + 2 \text{ M NaCl}$ solution in the presence and absence of 2 mM NaVO_3 at room temperature and $\text{pH} = 6.5$, using a Pt RDE at $\omega = 3000 \text{ RPM}$. The curves were recorded in the decreasing current direction.

at more negative potentials, reached at current densities higher than the limiting current density for the hypochlorite reduction (after the potential drop at $j \approx -130 \text{ mA cm}^{-2}$). This further indicates that the increased HER selectivity is caused by the deposited layer.

3.1.3. HER efficiency in hypochlorite and chlorate solutions

The effect of the sodium metavanadate addition on the HER efficiency in hypochlorite solutions was quantified by mass spectrometry

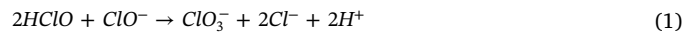
Fig. 1. (A) Cyclic voltammograms recorded at a sweep rate of $\nu = 10 \text{ mV s}^{-1}$ on a Pt RDE ($\omega = 3000 \text{ RPM}$) in an $80 \text{ mM NaOCl} + 2 \text{ M NaCl}$ solution at different NaVO_3 concentrations. (B) Cyclic voltammograms recorded at different sweep rates ($\nu = 5–100 \text{ mV s}^{-1}$) on a Pt RDE ($\omega = 3000 \text{ RPM}$) in an $80 \text{ mM NaOCl} + 2 \text{ M NaCl}$ solution, containing 2 mM NaVO_3 . The measurements were performed at room temperature and at $\text{pH} = 6.5$.

and galvanostatic measurements (Figs. S8 and 4 A). At low current density a small increase can be seen in the H_2 production-rate (and HER efficiency, accordingly) upon vanadate addition, which is more pronounced at higher current densities, i.e. large cathodic potentials (Fig. S8A). This can be explained by the results of the EQCM and polarization curve measurements: the vanadium oxide layer forms on the cathode at very negative potentials. The anodic oxygen by-product formation appears to be independent on the presence of vanadate (Fig. S8B), and the hypochlorite concentration did not change significantly during these measurements (Fig. S8C). This indicates, that this additive does not influence the anodic reactions and the homogeneous processes within these conditions.

At an industrially relevant current density of $j = -300 \text{ mA cm}^{-2}$ a gradual increase in the HER efficiency with the vanadate concentration was observed (Fig. 4A). At lower vanadate concentrations a slow HER efficiency increase indicates a sluggish layer build-up on the electrode, while at higher concentrations this process is significantly faster. Importantly, the current efficiency was above 95% in 2 mM NaVO_3 containing electrolytes (compared to 77% in the absence of this additive). Further, the effect of vanadate addition was tested for the electrochemical reduction of chlorate, which is another important loss reaction in the chlorate process, proceeding with fast kinetics on different oxide electrodes such as DSA (Fig. 4B). Again, a significantly increased (from 90% to $\sim 98\%$) HER efficiency was measured in the presence of 2 mM NaVO_3 .

3.1.4. Kinetic studies on the homogeneous decomposition of hypochlorite in bulk solutions

Beyond the electrochemical reactions, the formation of chlorate from the hypochlorite intermediate in the electrolyte bulk is also of importance for industrial chlorate production. In the absence of the vanadate additive in an electrolyte close to industrial composition (high ionic strength, $T = 80^\circ \text{C}$) chlorate formation (Eq. (1)) proceeds with high selectivity and oxygen forms in a smaller amount (Eq. (2), a competing loss reaction).



The rate of hypochlorite decomposition was not affected by addition of vanadate (Fig. 5A, decay curve), but the selectivity of the reaction towards oxygen formation increased (Fig. 5B); In the absence of vanadate, $\sim 5\%$ of the hypochlorite decomposed to oxygen, which increased to $\sim 10\%$ after adding 2 mM vanadate. As the increased oxygen formation is not only an efficiency loss, but also a safety concern as explosive gas mixtures may form in the chlorate cell (note that H_2 is produced on the cathode), finding a catalyst selective for chlorate formation is a prerequisite for applying the vanadate additive in industrial chlorate production.

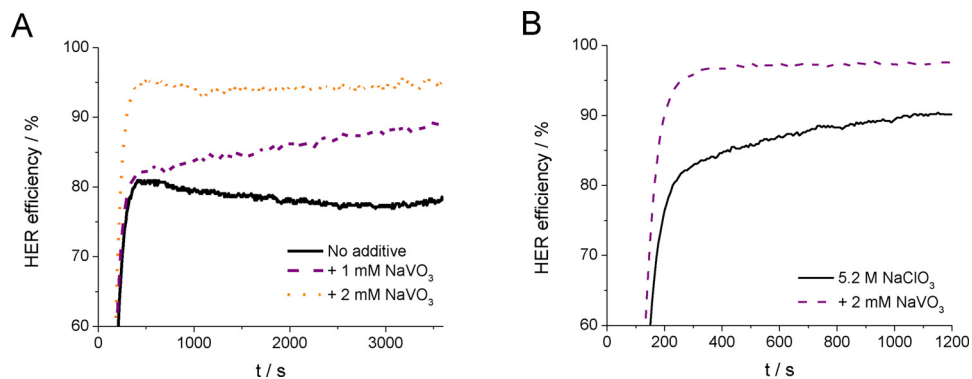


Fig. 4. HER efficiency measured at $j = -300 \text{ mA cm}^{-2}$ (A) using a Pt working electrode ($A = 1 \text{ cm}^2$) in $80 \text{ mM NaOCl} + 2 \text{ M NaCl}$ ($T = \text{room temperature}$, $\text{pH} = 6.5$) at different NaVO_3 concentrations, (B) on a ruthenium-oxide DSA working electrode in 5.2 M NaClO_3 solution at $T = 80^\circ\text{C}$, $\text{pH} = 6.5$.

3.2. General applicability of vanadate addition: Electrochemical selectivity

The effect of the vanadate addition and the subsequent deposition of a vanadium oxide film was further investigated for cathodic “loss” reactions (Fig. 6A–D), relevant for (photocatalytic) water splitting (preventing catalyst poisoning or the recombination of the products). First, the reduction of dissolved oxygen was studied (Figs. 6A and S9). In an oxygen saturated solution, a current plateau is seen from $E = -0.3 \text{ V}$, related to the diffusion limited oxygen reduction reaction (ORR) [52]. In the presence of vanadate a significantly reduced ORR current is seen in the anodic sweep. At $E \approx -0.35 \text{ V}$ the vanadium oxide dissolves, and an increased ORR current is observed at more positive potentials. Accordingly, when the oxidative dissolution of the layer was avoided by limited potential regions ($E < -0.5 \text{ V}$), ORR suppression was improved in the subsequent cycles (Fig. S9). Already after 3 cycles of layer buildup ORR was significantly suppressed.

Similarly, a significant hindering of the reduction of nitrate ions (Fig. 6B), hydrogen peroxide (Fig. 6C) and $\text{K}_3\text{Fe}(\text{CN})_6$ (Fig. 6D) was found during cyclic voltammetric measurements. It should be noted that all experiments were started from the cathodic endpoint of the potential window, hence deposition of the protecting vanadium oxide layer occurs at the beginning of the experiment. It is important to highlight, that these reactions are very different in nature. Most notably, the reduction of $\text{K}_3\text{Fe}(\text{CN})_6$ is a typical outer-sphere reaction. In this case – due to tunneling effect – the reaction proceeds even if the reactants cannot get closer than a few nm from the catalytic surface [18]. Thus, the thickness of the vanadium oxide coating deposited at negative electrode potentials must reach at least this thickness. When repeating the same experiments on a platinum electrode (Fig. S10), a less pronounced hindering was observed confirming that film formation is dependent on the electrode material, which is supported by the difference observed during EQCM measurements on Au or Pt-coated

electrodes. Importantly, applying a less positive anodic end-potential during potential cycling (avoiding the oxidative dissolution of the vanadium oxide layer), a suppressed ferricyanide reduction was observed in the whole potential range (Fig. S11).

In line with the polarization curve measurements (Fig. 3 and Fig. S6–7), where very similar Tafel-slopes were found in the presence and absence of vanadate these measurements strongly suggest that the HER proceeds on the electrode surface, at the interface between the substrate and the deposited coating and not on the surface of this latter. Hence the role of the deposited layer can most probably be found in the selective transport of different species. Vanadium oxides are therefore promising candidates for protection of either co-catalysts during photocatalytic water splitting, or catalysts during electrochemical water splitting, scenarios which are currently being studied in our laboratories.

4. Conclusions

Sodium metavanadate is a promising solution additive for processes in undivided electrochemical cells, inducing selective cathodic hydrogen evolution in various electrolytes, while the HER kinetics is not affected significantly. The hindering effect is caused by the in situ formation of a vanadium oxide film on the cathode during electrolysis. These results indicate that the hydrogen evolution proceeds at the interface between the electrode substrate and the vanadium oxide film.

The HER efficiency significantly increased upon vanadate addition both in hypochlorite and concentrated chlorate solutions. The unwanted anodic oxygen production rate was unaffected by the presence of vanadate, whereas the rate of oxygen evolution from homogeneous hypochlorite decomposition increased, requiring an alternative additive to promote conversion of hypochlorite to chlorate.

Further, the in situ formed vanadium oxide film hinders the

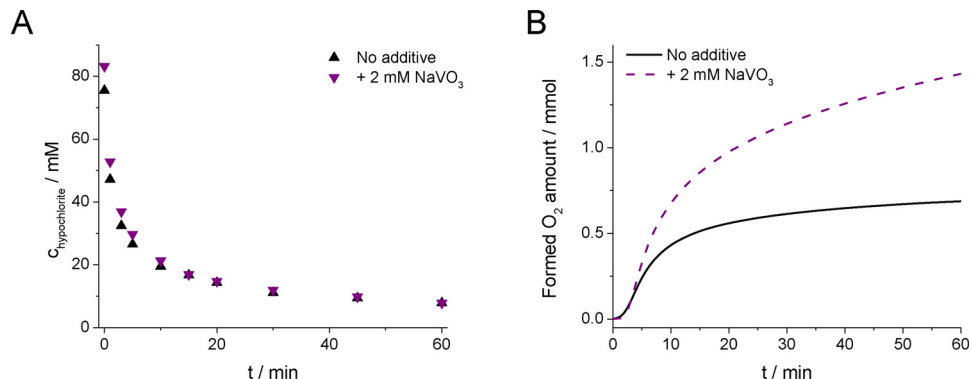


Fig. 5. (A) Hypochlorite concentration decay curves, (B) total amount of oxygen formed during the decomposition of hypochlorite from a $5.2 \text{ M NaClO}_3 + 1.9 \text{ M NaCl} + 80 \text{ mM NaClO}$ solution at $T = 80^\circ\text{C}$ and $\text{pH} = 6.5$.

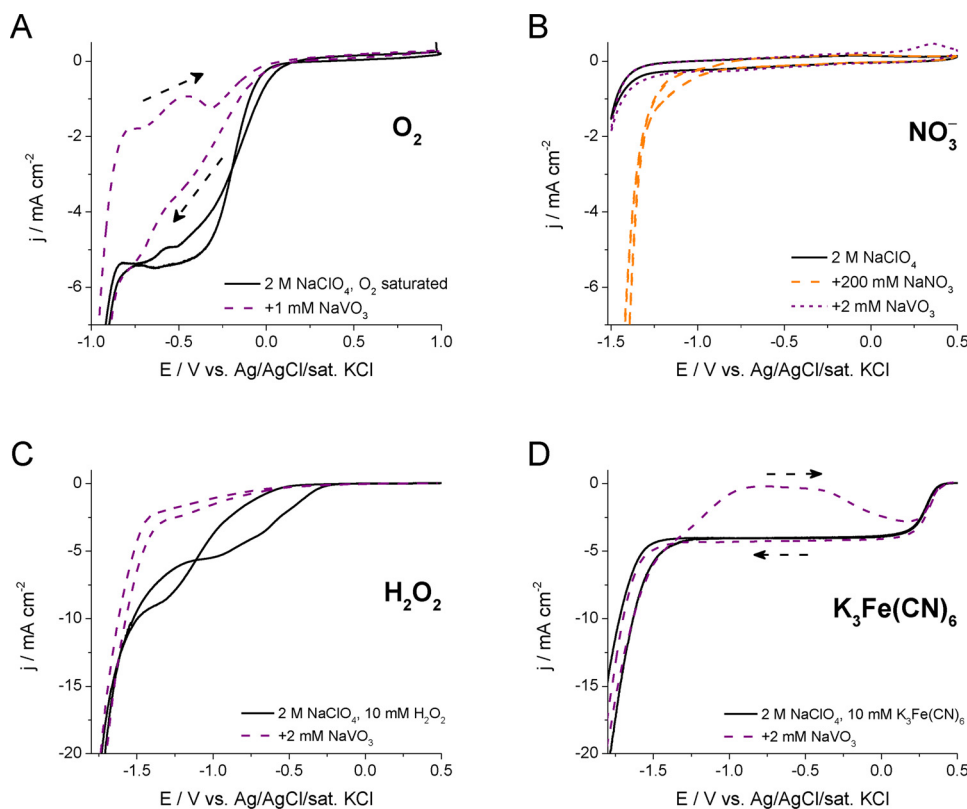


Fig. 6. (A) Cyclic voltammograms recorded on a Pt RDE ($\nu = 10 \text{ mV s}^{-1}$, $\omega = 3000 \text{ RPM}$) in a 2 M NaClO_4 solution saturated with argon or oxygen, w/wo the addition of 1 mM NaVO_3 . (B)-(D) Cyclic voltammograms recorded on a glassy carbon RDE ($\omega = 1000 \text{ RPM}$) in a N_2 purged 2 M NaClO_4 solution w/wo the addition of 2 mM NaVO_3 , in the presence of (B) 0.3 M NaNO_3 ($\nu = 100 \text{ mV s}^{-1}$) (C) 10 mM H_2O_2 ($\nu = 10 \text{ mV s}^{-1}$), (D) 10 mM $\text{K}_3\text{Fe}(\text{CN})_6$ ($\nu = 10 \text{ mV s}^{-1}$). All the curves were recorded in room temperature, pH = 6.5 solutions. The measurements were started from the cathodic endpoint, and for all experiments the 2nd cycle is shown.

reduction of nitrate ions, hydrogen peroxide, $\text{K}_3\text{Fe}(\text{CN})_6$ and dissolved oxygen as well. Such coatings can therefore be candidates for protective coatings to prevent catalyst poisoning or the recombination of the reaction products in the case electrochemical and photocatalytic water splitting.

Author contributions

The manuscript was written through contributions of all authors. All authors have given approval to the final version of the manuscript.

Acknowledgment

The financial support from the Swedish Energy Agency and Nouryon is gratefully acknowledged.

Appendix A. Supplementary data

Supplementary material related to this article can be found, in the online version, at doi:<https://doi.org/10.1016/j.apcatb.2018.11.038>.

References

- [1] M.S. Dresselhaus, I.L. Thomas, Alternative energy technologies, *Nature*. 414 (2001) 332–337, <https://doi.org/10.1038/35104599>.
- [2] E.V. Kondratenko, G. Mul, J. Baltrusaitis, G.O. Larrazábal, J. Pérez-Ramírez, Status and perspectives of CO_2 conversion into fuels and chemicals by catalytic, photocatalytic and electrocatalytic processes, *Energy Environ. Sci.* 6 (2013) 3112, <https://doi.org/10.1039/c3ee41272e>.
- [3] B. Endrődi, G. Benesik, F. Darvas, R. Jones, K. Rajeshwar, C. Janáky, Continuous-flow electroreduction of carbon dioxide, *Prog. Energy Combust. Sci.* 62 (2017) 133–154, <https://doi.org/10.1016/j.pecs.2017.05.005>.
- [4] N.S.N. Lewis, D.D.G. Nocera, Powering the planet: chemical challenges in solar energy utilization, *Proc. Natl. Acad. Sci. U. S. A.* 103 (2006) 15729–15735, <https://doi.org/10.1073/pnas.0603395103>.
- [5] K. Maeda, K. Domen, Photocatalytic Water Splitting: Recent Progress and Future Challenges, *J. Phys. Chem. Lett.* 1 (2010) 2655–2661, <https://doi.org/10.1021/jz1007966>.
- [6] T. Hisatomi, J. Kubota, K. Domen, Recent advances in semiconductors for photocatalytic and photoelectrochemical water splitting, *Chem. Soc. Rev.* 43 (2014) 7520–7535, <https://doi.org/10.1039/C3CS60378D>.
- [7] G.W. Busser, B. Mei, P. Weide, P.C.K. Vesborg, K. Stihrenberg, M. Bauer, X. Huang, M.-G. Willinger, I. Chorkendorff, R. Schlögl, M. Muhler, Cocatalyst designing: a regenerable molybdenum-containing ternary cocatalyst system for efficient photocatalytic water splitting, *ACS Catal.* 5 (2015) 5530–5539, <https://doi.org/10.1021/acscatal.5b01428>.
- [8] D. Eisenberg, H.S. Ahn, A.J. Bard, Enhanced photoelectrochemical water oxidation on bismuth vanadate by electrodeposition of amorphous titanium dioxide, *J. Am. Chem. Soc.* 136 (2014) 14011–14014, <https://doi.org/10.1021/ja5082475>.
- [9] K. Han, T. Kreuger, B. Mei, G. Mul, Transient behavior of $\text{Ni}@\text{NiO}$ functionalized SrTiO_3 in overall water splitting, *ACS Catal.* 7 (2017) 1610–1614, <https://doi.org/10.1021/acscatal.6b03662>.
- [10] Y. Matsumoto, U. Unal, N. Tanaka, A. Kudo, H. Kato, Electrochemical approach to evaluate the mechanism of photocatalytic water splitting on oxide photocatalysts, *J. Solid State Chem.* 177 (2004) 4205–4212, <https://doi.org/10.1016/j.jssc.2004.08.001>.
- [11] G. Yuan, A. Agiral, N. Pellet, W. Kim, H. Frei, Inorganic core–shell assemblies for closing the artificial photosynthetic cycle, *Faraday Discuss.* 176 (2014) 233–249, <https://doi.org/10.1039/C4FD00150H>.
- [12] J.A. Bau, K. Takanabe, Ultrathin microporous SiO_2 membranes photodeposited on hydrogen evolving catalysts enabling overall water splitting, *ACS Catal.* 7 (2017) 7931–7940, <https://doi.org/10.1021/acscatal.7b03017>.
- [13] N.Y. Labrador, E.L. Songcuan, C. De Silva, H. Chen, S.J. Kudziel, R.K. Ramachandran, C. Detavernier, D.V. Esposito, Hydrogen evolution at the buried interface between Pt thin films and silicon oxide nanomembranes, *ACS Catal.* 8 (2018) 1767–1778, <https://doi.org/10.1021/acscatal.7b02668>.
- [14] A.T. Garcia-Esparza, T. Shinagawa, S. Ould-Chikha, M. Qureshi, X. Peng, N. Wei, D.H. Anjum, A. Clo, T.-C. Weng, D. Nordlund, D. Sokaras, J. Kubota, K. Domen, K. Takanabe, An oxygen-insensitive hydrogen evolution catalyst coated by a molybdenum-based layer for overall water splitting, *Angew. Chem. Int. Ed.* 56 (2017) 5780–5784, <https://doi.org/10.1002/anie.201701861>.
- [15] M. Yoshida, K. Takanabe, K. Maeda, A. Ishikawa, J. Kubota, Y. Sakata, Y. Ikezawa, K. Domen, Role and function of noble-metal/Cr-layer core/shell structure cocatalysts for photocatalytic overall water splitting studied by model electrodes, *J. Phys. Chem. C* 113 (2009) 10151–10157, <https://doi.org/10.1021/jp901418u>.
- [16] K. Maeda, K. Teramura, D. Lu, N. Saito, Y. Inoue, K. Domen, Noble-metal/Cr₂O₃ core/shell nanoparticles as a cocatalyst for photocatalytic overall water splitting, *Angew. Chem. Int. Ed.* 45 (2006) 7806–7809, <https://doi.org/10.1002/anie.200602473>.
- [17] K. Maeda, K. Teramura, D. Lu, N. Saito, Y. Inoue, K. Domen, Roles of Rh/Cr₂O₃(Core/Shell) nanoparticles photodeposited on visible-light-responsive (Ga_{1-x}Zn_x)(N_{1-x}O_x) solid solutions in photocatalytic overall water splitting, *J. Phys. Chem. C* 111 (2007) 7554–7560, <https://doi.org/10.1021/jp071056j>.
- [18] M. Qureshi, T. Shinagawa, N. Tsiaapis, K. Takanabe, Exclusive hydrogen generation by electrocatalysts coated with an amorphous chromium-based layer achieving

efficient overall water splitting, *ACS Sustain. Chem. Eng.* 5 (2017) 8079–8088, <https://doi.org/10.1021/acssuschemeng.7b01704>.

[19] D.V. Esposito, Membrane-coated electrocatalysts—an alternative approach to achieving stable and tunable electrocatalysis, *ACS Catal.* 8 (2018) 457–465, <https://doi.org/10.1021/acscatal.7b03374>.

[20] J.G. Vos, T.A. Wezendonk, A.W. Jeremiassse, M.T.M. Koper, $\text{MnO}_x/\text{IrO}_x$ as selective oxygen evolution electrocatalyst in acidic chloride solution, *J. Am. Chem. Soc.* 140 (2018) 10270–10281, <https://doi.org/10.1021/jacs.8b05382>.

[21] J.E. Colman, B.V. Tilak, Sodium chlorate, in: J.J. McKetta, G.E. Weismantel (Eds.), *Encycl. Chem. Process. Des. Vol. 51 - Slurry Syst. Instrum. to Solid-Liquid Sep.* Marcel Dekker Inc., 1995, pp. 126–186.

[22] A. Cornell, *Encyclopedia of Applied Electrochemistry*, Springer, New York, New York, NY, 2014, <https://doi.org/10.1007/978-1-4419-6996-5>.

[23] H. Vogt, Electrosynthesis of chlorate in the nineteenth century, *J. Electrochem. Soc.* 128 (1981) 29C, <https://doi.org/10.1149/1.2127407>.

[24] B. Endrődi, N. Simic, M. Wildlock, A. Cornell, A review of chromium(VI) use in chlorate electrolysis: Functions, challenges and suggested alternatives, *Electrochim. Acta* 234 (2017) 108–122, <https://doi.org/10.1016/j.electacta.2017.02.150>.

[25] A. Cornell, G. Lindbergh, D. Simonsson, The effect of addition of chromate on the hydrogen evolution reaction and on iron oxidation in hydroxide and chlorate solutions, *Electrochim. Acta* 37 (1992) 1873–1881, [https://doi.org/10.1016/0013-4686\(92\)85093-Z](https://doi.org/10.1016/0013-4686(92)85093-Z).

[26] A. Ahlberg Tidblad, G. Lindbergh, Surface analysis with ESCA and GD-OES of the film formed by cathodic reduction of chromate, *Electrochim. Acta* 36 (1991) 1605–1610, [https://doi.org/10.1016/0013-4686\(91\)85013-W](https://doi.org/10.1016/0013-4686(91)85013-W).

[27] G. Lindbergh, D. Simonsson, Inhibition of cathode reactions in sodium hydroxide solution containing chromate, *Electrochim. Acta* 36 (1991) 1985–1994, [https://doi.org/10.1016/0013-4686\(91\)85083-J](https://doi.org/10.1016/0013-4686(91)85083-J).

[28] I. Taniguchi, T. Sekine, The influence of chromate addition on the cathodic reduction of hypochlorite ion, *Denki Kagaku* 43 (1975) 201–208.

[29] G. Lindbergh, D. Simonsson, The effect of chromate addition on cathodic reduction of hypochlorite in hydroxide and chlorate solutions, *J. Electrochem. Soc.* 137 (1990) 3094, <https://doi.org/10.1149/1.2086165>.

[30] G. Ilevbare, G. Burstein, The inhibition of pitting corrosion of stainless steels by chromate and molybdate ions, *Corros. Sci.* 45 (2003) 1545–1569, [https://doi.org/10.1016/S0010-938X\(02\)00229-9](https://doi.org/10.1016/S0010-938X(02)00229-9).

[31] A.A. Tidblad, J. Martensson, In situ ellipsometric characterization of films formed by cathodic reduction of chromate, *Electrochim. Acta* 42 (1997) 389–398, [https://doi.org/10.1016/S0013-4686\(96\)00229-0](https://doi.org/10.1016/S0013-4686(96)00229-0).

[32] J.W. Ball, D.K. Nordstrom, Critical evaluation and selection of standard state thermodynamic properties for chromium metal and its aqueous ions, hydrolysis species, oxides, and hydroxides, *J. Chem. Eng. Data* 43 (1998) 895–918, <https://doi.org/10.1021/je980080a>.

[33] M. Spasojević, D. Marković, T. Trišović, M. Spasojević, Mathematical model of the catalytic effect of chromium(VI) on hypochlorite disproportionation in chlorate electrolysis, *J. Electrochem. Soc.* 165 (2018) E8–E19, <https://doi.org/10.1149/2.0291802jes>.

[34] J. Wanngård, M. Wildlock, The catalyzing effect of chromate in the chlorate formation reaction, *Chem. Eng. Res. Des.* 121 (2017) 438–447, <https://doi.org/10.1016/j.cherd.2017.03.021>.

[35] J. Kalmár, M. Szabó, N. Simic, I. Fábián, Kinetics and mechanism of the chromium (VI) catalyzed decomposition of hypochlorous acid at elevated temperature and high ionic strength, *Dalton Trans.* 47 (2018) 3831–3840, <https://doi.org/10.1039/C8DT00120K>.

[36] J. Gustavsson, L. Nylén, A. Cornell, Rare earth metal salts as potential alternatives to Cr(VI) in the chlorate process, *J. Appl. Electrochem.* 40 (2010) 1529–1536, <https://doi.org/10.1007/s10800-010-0136-4>.

[37] M. Li, Z. Twardowski, F. Mok, N. Tam, Sodium molybdate—a possible alternate additive for sodium dichromate in the electrolytic production of sodium chlorate, *J. Appl. Electrochem.* 37 (2007) 499–504, <https://doi.org/10.1007/s10800-006-9281-1>.

[38] J. Gustavsson, G. Li, C. Hummelgard, J. Backstrom, A. Cornell, On the suppression of cathodic hypochlorite reduction by electrolyte additions of molybdate and chromate ions, *J. Electrochem. Sci. Eng.* 2 (2012) 185–198, <https://doi.org/10.5599/jese.2012.0021>.

[39] J. Gustavsson, C. Hummelgard, J. Backstrom, I.O. Wallinder, S.M. Rahman, G. Lindbergh, S. Eriksson, A. Cornell, In-situ activated hydrogen evolution by molybdate addition to neutral and alkaline electrolytes, *J. Electrochem. Sci. Eng.* 2 (2012) 105–120, <https://doi.org/10.5599/jese.2012.0015>.

[40] B. Endrődi, S. Sandin, V. Smulders, N. Simic, M. Wildlock, G. Mul, B.T. Mei, A. Cornell, Towards sustainable chlorate production: the effect of permanganate addition on current efficiency, *J. Clean. Prod.* 182 (2018) 529–537, <https://doi.org/10.1016/j.jclepro.2018.02.071>.

[41] L. Su, J.A. Kowalski, K.J. Carroll, F.R. Brushett, Recent developments and trends in redox flow batteries, *Electron. Commun. Eng. J.* (2015) 673–712, https://doi.org/10.1007/978-3-319-15458-9_24.

[42] P. Leung, X. Li, C. Ponce de León, L. Berlouis, C.T.J. Low, F.C. Walsh, Progress in redox flow batteries, remaining challenges and their applications in energy storage, *RSC Adv.* 2 (2012) 10125, <https://doi.org/10.1039/c2ra21342g>.

[43] Z. Zou, N. Li, D. Li, H. Liu, S. Mu, A vanadium-based conversion coating as chromate replacement for electrogalvanized steel substrates, *J. Alloys. Compd.* 509 (2011) 503–507, <https://doi.org/10.1016/j.jallcom.2010.09.080>.

[44] V.G. Sribharathy, S. Rajendran, Corrosion inhibition of carbon steel by sodium metavanadate, *J. Electrochem. Sci. Eng.* 2 (2012) 121–131, <https://doi.org/10.5599/jese.2012.0014>.

[45] K.D. Ralston, S. Chrisanti, T.L. Young, R.G. Buchheit, Corrosion inhibition of aluminum alloy 2024-T3 by aqueous vanadium species, *J. Electrochem. Soc.* 155 (2008) C350, <https://doi.org/10.1149/1.2907772>.

[46] M. Zhang, J.R. Dahn, Electrochemical lithium intercalation in $\text{VO}_2(\text{B})$ in aqueous electrolytes, *J. Electrochem. Soc.* 143 (1996) 2730, <https://doi.org/10.1149/1.1837099>.

[47] J.G. Chen, C.W. Jones, S. Linic, V.R. Stamenkovic, Best practices in pursuit of topics in heterogeneous electrocatalysis, *ACS Catal.* 7 (2017) 6392–6393, <https://doi.org/10.1021/acscatal.7b02839>.

[48] C. Hummelgård, R.K.B. Karlsson, J. Bäckström, S.M.H. Rahman, A. Cornell, S. Eriksson, H. Olin, Physical and electrochemical properties of cobalt doped (Ti, Ru) O_2 electrode coatings, *Mater. Sci. Eng. B* 178 (2013) 1515–1522, <https://doi.org/10.1016/j.mseb.2013.08.018>.

[49] B. Liu, S. Zheng, S. Wang, Y. Zhang, A. Ortega, N.S. Kim, K. Han, H. Du, The redox behavior of vanadium in alkaline solutions by cyclic voltammetry method, *Electrochim. Acta* 76 (2012) 262–269, <https://doi.org/10.1016/j.electacta.2012.05.008>.

[50] V.I. Birss, M. Chang, J. Segal, Platinum oxide film formation—reduction: an in-situ mass measurement study, *J. Electroanal. Chem. Lausanne (Lausanne)* 355 (1993) 181–191, [https://doi.org/10.1016/0022-0728\(93\)80361-K](https://doi.org/10.1016/0022-0728(93)80361-K).

[51] M.C. Biesinger, B.P. Payne, A.P. Grosvenor, L.W.M. Lau, A.R. Gerson, R.S.C. Smart, Resolving surface chemical states in XPS analysis of first row transition metals, oxides and hydroxides: Cr, Mn, Fe, Co and Ni, *Appl. Surf. Sci.* 257 (2011) 2717–2730, <https://doi.org/10.1016/j.apsusc.2010.10.051>.

[52] U.A. Paulus, T.J. Schmidt, H.A. Gasteiger, R.J. Behm, Oxygen reduction on a high-surface area Pt/Vulcan carbon catalyst: a thin-film rotating ring-disk electrode study, *J. Electroanal. Chem. Lausanne (Lausanne)* 495 (2001) 134–145, [https://doi.org/10.1016/S0022-0728\(00\)00407-1](https://doi.org/10.1016/S0022-0728(00)00407-1).